

Alignment-Free RGB-T Salient Object Detection: A Large-scale Dataset and Progressive Correlation Network

Kunpeng Wang¹, Keke Chen¹, Chenglong Li², Zhengzheng Tu^{1*}, Bin Luo^{1*}

¹Key Laboratory of Intelligent Computing and Signal Processing of Ministry of Education, Anhui Provincial Key Laboratory of Multimodal Cognitive Computation, School of Computer Science and Technology, Anhui University, China

²Anhui Provincial Key Laboratory of Security Artificial Intelligence, School of Artificial Intelligence, Anhui University, China
{kp.wang, chen1220, lcl1314}@foxmail.com, zhengzhengahu@163.com, luobin@ahu.edu.cn

Abstract

Alignment-free RGB-Thermal (RGB-T) salient object detection (SOD) aims to achieve robust performance in complex scenes by directly leveraging the complementary information from unaligned visible-thermal image pairs, without requiring manual alignment. However, the labor-intensive process of collecting and annotating image pairs limits the scale of existing benchmarks, hindering the advancement of alignment-free RGB-T SOD. In this paper, we construct a large-scale and high-diversity unaligned RGB-T SOD dataset named UVT20K, comprising 20,000 image pairs, 407 scenes, and 1256 object categories. All samples are collected from real-world scenarios with various challenges, such as low illumination, image clutter, complex salient objects, and so on. To support the exploration for further research, each sample in UVT20K is annotated with a comprehensive set of ground truths, including saliency masks, scribbles, boundaries, and challenge attributes. In addition, we propose a Progressive Correlation Network (PCNet), which models inter- and intra-modal correlations on the basis of explicit alignment to achieve accurate predictions in unaligned image pairs. Extensive experiments conducted on unaligned and aligned datasets demonstrate the effectiveness of our method.

Code and Dataset — <https://github.com/Angknpng/PCNet>

Introduction

Salient object detection (SOD) aims to identify and segment the most attractive regions in visual scenes. It can help eliminate redundant information and has been applied in a variety of vision tasks, such as image compression (Li et al. 2017), video analysis (Fan et al. 2019), and visual tracking (Zhang et al. 2020). Although great progress has been made, RGB SOD methods (Wang et al. 2022) only based on visible images still struggle to distinguish salient regions in complex scenes, such as background clutter, low illumination, and similar foreground and background.

Thermal sensors can capture the overall shape of objects, providing complementary information to visible images (Lu et al. 2021; Zhu et al. 2021; Yuan et al. 2024). Therefore, some studies introduce thermal images alongside visible images to enhance performance in complex

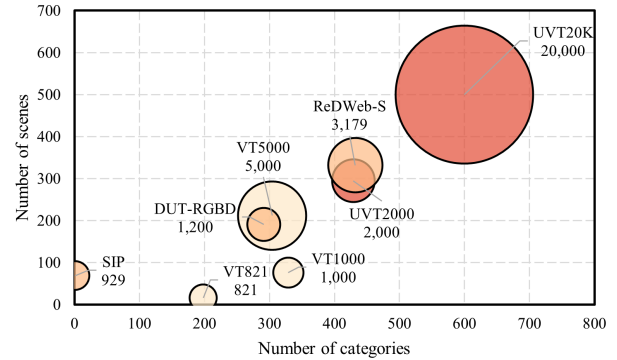


Figure 1: Comparison on scale (i.e., circular area), scenes (i.e., vertical axis), and object categories (i.e., horizontal axis) of the proposed UVT20K dataset with existing representative RGB-T and RGB-D SOD datasets, including UVT2000 (Wang et al. 2024a), VT5000 (Tu et al. 2020), VT1000 (Tu et al. 2019), VT821 (Wang et al. 2018), ReDWeb-S (Liu et al. 2021a), SIP (Fan et al. 2020), and DUT-RGBD (Piao et al. 2019).

scenes. For example, (Tu et al. 2020) release a prevalent RGB-Thermal (RGB-T) SOD benchmark with spatial alignment to facilitate the utilization of corresponding multi-modal information. Therefore, existing methods are almost designed on the basis of alignment, and demonstrate their effectiveness through modality discrepancy reduction (Liu et al. 2021c), multi-modal interaction improvement (Tu et al. 2021), modality modulation (Cong et al. 2022), and so on.

However, the original captured RGB-T image pairs are unaligned in space and scale, and manually aligning them is labor-intensive and not conducive to practical application and deployment. Moreover, directly applying existing alignment-based methods to unaligned data leads to significant performance degradation due to the difficulty of exploiting multi-modal correspondences. To this end, (Tu et al. 2022) make the first attempt to build modality correspondences on weakly aligned datasets, which are artificially created from existing aligned datasets (Wang et al. 2018; Tu et al. 2019, 2020) by spatial affine transformation. While the weakly aligned datasets contribute positively to the ad-

*Corresponding authors.

vancement of SOD, they still fall short of meeting practical application requirements. In addition, the local correspondences established through convolutional operations are insufficient to handle large spatial deviations that occur in real-world misalignment. Recently, (Wang et al. 2024a) release the first unaligned dataset (i.e., UVT2000) and design a correlation modeling method based on asymmetric window pairs. Nonetheless, two issues still exist: 1) UVT2000 is limited in scale as it only contains 2,000 unaligned image pairs for testing and lacks a training set for models to learn the properties of unaligned data, 2) the fixed-size asymmetric window pairs cannot flexibly adjust their shapes according to the misalignment status in different scenes, failing to cover the complete corresponding multi-modal information.

To address the first issue, we construct a large-scale unaligned RGB-T SOD benchmark named UVT20K with multiple characteristics. Firstly, to the best of our knowledge, UVT20K is the largest multi-modal SOD dataset containing 20,000 unaligned image pairs with both training and testing sets. It will play an important role in training and evaluating alignment-free RGB-T SOD methods. Secondly, UVT20K covers 407 scenes, 1256 object categories, and 15 kinds of challenges, endowing it with a high degree of diversity and complexity. Thirdly, each sample in UVT20K is annotated with a comprehensive set of ground truths, including saliency masks, scribbles, boundaries, and challenge attributes, which provide a foundation for extensive research. As shown in Fig. 1, UVT20K is far beyond recent representative multi-modal datasets in terms of scale, scene, and object category. Notably, we include both RGB-T and RGB-Depth (RGB-D) datasets for a comprehensive comparison.

To address the second issue, we propose a Progressive Correlation Network (PCNet) that models inter- and intra-modal correlations on the basis of explicit alignment. To be specific, we propose a Semantics-guided Homography Estimation (SHE) module that introduces and fine-tunes an existing multi-modal homography estimator (Cao et al. 2022) to explicitly align the common regions between RGB and thermal modalities. Considering that the estimator is pre-trained on other multi-modal datasets, we design an S-Adapter to adapt it to RGB-T data. Meanwhile, semantic information is embedded into S-Adapter to guide the estimator to predict the homography matrix against object regions. Since only the overlapping multi-modal regions will be aligned in unaligned image pairs, it is difficult to model the correlation of complete saliency regions with multi-modal fusion alone. To this end, we also propose an Inter- and Intra-Modal Correlation (IIMC) module to fully model the correlation of salient regions. IIMC first models the multi-modal correlation of the corresponding partial region, and then expands the correlation to the entire region within the modality. In this way, correlations of salient objects can be modeled progressively to achieve accurate saliency predictions. The main contributions of our work are as follows:

- We construct a large-scale benchmark dataset named UVT20K for alignment-free RGB-T SOD. To the best of our knowledge, UVT20K is the largest multi-modal SOD dataset, containing 20,000 unaligned visible-thermal image pairs, covering 407 scenes and 1256 object categories

with 15 challenges, providing a comprehensive set of annotations. Our dataset will be available to the research community for extensive investigation and exploration.

- We propose a Progressive Correlation Network (PCNet) that explores and integrates saliency cues in unaligned RGB-T image pairs to achieve accurate predictions.
- We propose a semantics-guided homography estimation module to explicitly align corresponding multi-modal regions, and an inter- and intra-modal correlation module to progressively model correlations for salient objects.
- We conduct a comprehensive evaluation of state-of-the-art methods and an in-depth experimental analysis of our PCNet on the newly constructed benchmark dataset, as well as the other aligned and unaligned datasets.

Related Work

RGB-T Salient Object Detection Benchmarks

The first dataset for RGB-T Salient Object Detection (SOD) is VT821 (Wang et al. 2018), which contains 821 pairs of images collected from a recording system consisting of a thermal imager (i.e., FLIR A310) and a CCD camera (i.e., SONY TD-2073). All 821 image pairs are manually aligned using point correspondences and annotated with saliency masks and challenge attributes. Then, VT1000 (Tu et al. 2019) enlarges the scale to 1,000 manually aligned and annotated image pairs, which are captured by the FLIR SC620 device with a thermal infrared camera and a CCD camera inside. Later, VT5000 (Tu et al. 2020) was built with 5,000 image pairs captured by the FLIR T640 device. The aligned samples in VT5000 are divided into two halves, each containing 2,500 samples for the training and testing. These aligned datasets provide the foundation for alignment-based methods, however, the labor-intensive manual alignment is not conducive to practical application and deployment.

To overcome this problem, (Tu et al. 2022) artificially create the corresponding weakly aligned datasets (i.e., un-VT821, un-VT1000, and un-VT5000) by performing random affine transformations on the above three aligned datasets. Recently, (Wang et al. 2024a) release the UVT2000 dataset with 2,000 unaligned image pairs captured by a FLIR SC620 device without manual alignment. However, UVT2000 is small in scale and lacks a training set, preventing the corresponding methods from learning the properties of unaligned image pairs and limiting the research on alignment-free RGB-T SOD. To this end, we construct a large-scale unaligned dataset consisting of 20,000 image pairs, which contain a training set and a test set, rich scenes and object categories, and a variety of annotations.

RGB-T Salient Object Detection Methods

RGB-T salient object detection focuses on fusing information from RGB and thermal modalities to predict their common salient regions. Based on the aligned benchmark datasets, enormous methods have been presented through graph learning (Tang et al. 2019; Tu et al. 2019), multi-scale feature interaction (Wang et al. 2021; Tu et al. 2021), lightweight design (Huo et al. 2021, 2022; Zhou et al. 2023),

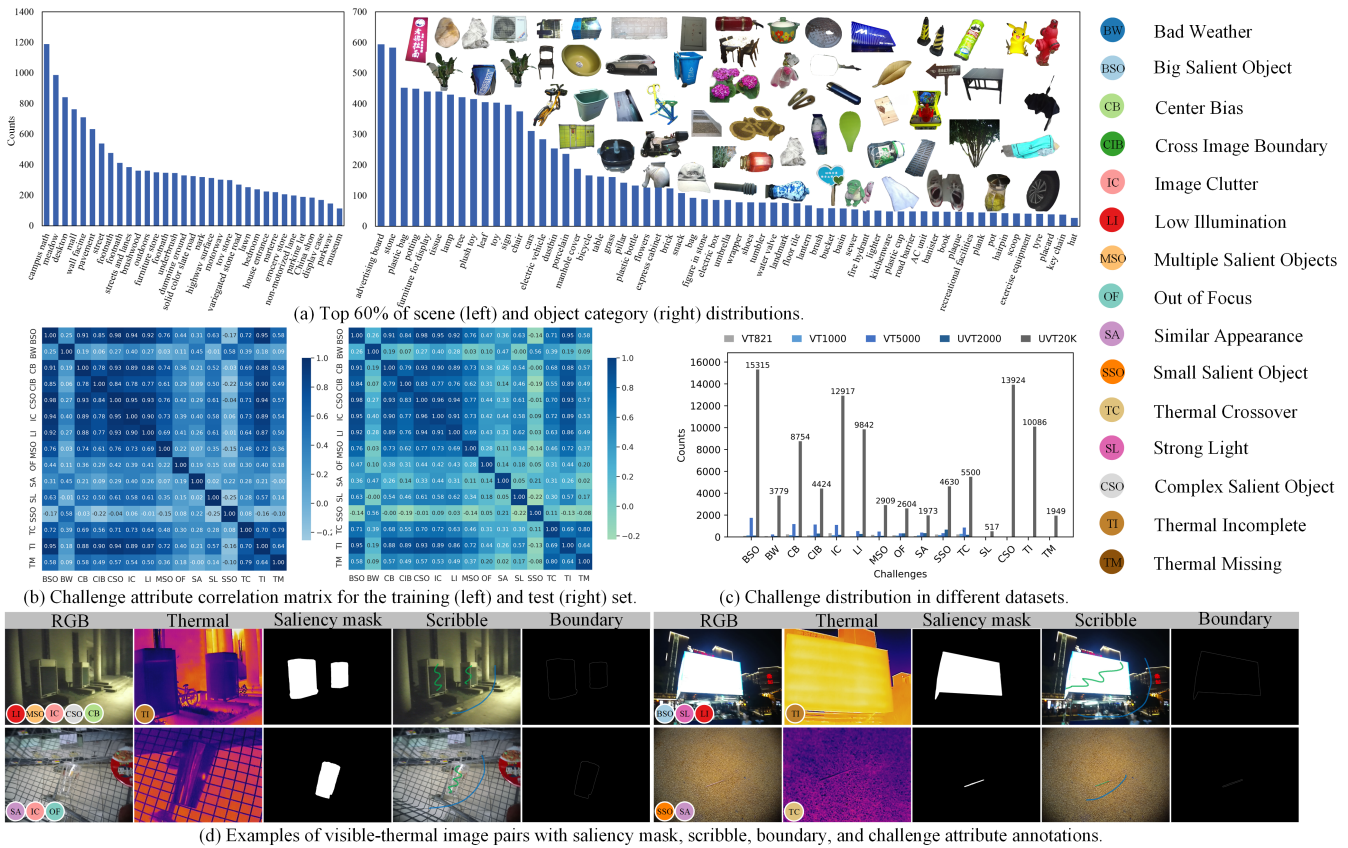


Figure 2: Main statistics and characteristics of our UVT20K dataset.

global information modeling (Liu et al. 2021c; Tang et al. 2022; Pang et al. 2023), and ensemble learning (Wang et al. 2024b). Although great progress has been made, these methods rely on the corresponding spatial information in modality alignment. Therefore, it is difficult for them to capture the correlated information in unaligned image pairs.

DCNet (Tu et al. 2022) attempts to establish multi-modal correspondences in weakly aligned image pairs via affine transformation and dynamic convolution. Although effective in weakly aligned image pairs with small spatial offsets, the local receptive fields of the convolutional operation have difficulty in handling large deviations in space and scale. To improve it, SACNet (Wang et al. 2024a) uses a pair of asymmetric windows to cover the corresponding information in unaligned image pairs. However, the fixed windows fail to flexibly cover the corresponding information for different scenes, leading to the introduction of unrelated noise for correlation modeling. In this paper, we explicitly align the common information of the two modalities and progressively model inter- and intra-modal correlations.

UVT20K Benchmark

Existing RGB-T SOD datasets (Wang et al. 2018; Tu et al. 2019, 2020) are almost manually aligned and labor-intensive, while the only unaligned dataset (Wang et al. 2024a) is limited in scale and lacks a training set, which re-

stricts the research on alignment-free RGB-T SOD. To address this issue, we construct a large-scale and high-diversity unaligned RGB-T SOD dataset denoted as UVT20K.

Dataset Construction

Dataset Collection. The proposed UVT20K dataset is captured in the real world using Hikvision DS-2TP23-10VF/W(B) and FLIR SC620 devices, which are equipped with a pair of CCD and thermal infrared cameras. Each sample is directly obtained by camera shot without manual alignment. Although integrated in a single device, the CCD and thermal infrared camera pairs have parallax and different viewing angle sizes. Therefore, the same object captured by both devices suffers from positional offsets and scale differences, resulting in misalignment.

Dataset Annotation. We first perform a quality scan on the initially captured 24,000+ image pairs to remove duplicate, objectless, and corrupted samples. Then, the rest 22,000+ high-quality image pairs are delivered to ten annotators, who select and annotate the most attractive objects or regions at the first glance. Based on the majority voting for salient objects, we rank and select the top 20,000 annotated samples as the final dataset. Note that the annotation process is based on the human-preferred RGB images, with the corresponding thermal images used for assistance. In addition, we annotate each sample with scribbles and boundaries, which can

Dataset	Year	Modality			Scene Number	Category Number	Alignment Status	Practical Shooting	Training Subset	Weak Annotation	Boundary Annotation	Challenge Annotation	Challenge Number	Image Source	
		RGB	Thermal	Depth											
DUTLF-Depth	2019	1200	-	1200	191	291	Aligned	✓	✓	×	×	×	-	By Lytro camera By mobile phone From ReDWeb dataset	
SIP	2020	929	-	929	69	1	Aligned	✓	×	×	×	×	-		
ReDWeb-S	2021	3,179	-	3,179	332	432	Aligned	×	×	×	×	×	-		
VT821	2018	821	821	-	16	198	Aligned	✓	×	×	×	✓	11	By FLIR camera By FLIR camera By FLIR camera From VT821 dataset From VT1000 dataset From VT5000 dataset By FLIR camera	
VT1000	2019	1,000	1,000	-	76	329	Aligned	✓	×	×	×	✓	10		
VT5000	2020	5,000	5,000	-	212	304	Aligned	✓	✓	×	×	✓	11		
un-VT821	2022	821	821	-	16	198	Weakly aligned	×	×	×	×	×	-		
un-VT1000	2022	1,000	1,000	-	76	329	Weakly aligned	×	×	×	×	×	-		
un-VT5000	2022	5,000	5,000	-	212	304	Weakly aligned	×	×	×	×	×	-		
UVT2000	2024	2,000	2,000	-	295	429	Unaligned	✓	×	×	×	✓	11		
UVT20K (Ours)	-	20,000	20,000	-	407	1256	Unaligned	✓	✓	✓	✓	✓	15		By Hikvision and FLIR cameras

Table 1: Comparison of UVT20K with prevalent multi-modal SOD datasets.

be used for weak supervision and other related studies. To facilitate subsequent work on challenging scenes, we also annotate each sample with one or more challenge attributes. A total of 15 challenge attributes are listed on the right side of Fig.2, in which the first 11 challenge attributes are derived from existing RGB-T datasets (Tu et al. 2020) and the last four new challenges (i.e., SL, CSO, TI, TC) are summarized and added for UVT20K. In particular, TI is the case where salient objects are not completely captured in thermal images, and TC is the extreme case of TI. Some visual examples from our dataset are illustrated in Fig. 2(d). Due to space limitations, more examples are provided in *supp*.

Dataset Splits. Following the representative RGB-T SOD dataset VT5000 (Tu et al. 2020), we randomly select 10,000 pairs of images in UVT20K dataset as the training set, and take the remaining 10,000 pairs as the test set. Fig. 2(b) illustrates the challenge attribute correlation matrix for the training and test sets. A higher correlation between two challenge attributes in the matrix indicates a higher probability of their co-existence. The similar challenge distributions validate the rationality of the dataset splits and facilitate the accurate evaluation of various models.

Dataset Comparisons and Characteristics

As shown in Table 1, compared with prevalent multi-modal SOD datasets, UVT20K has the following characteristics.

- UVT20K contains a vast collection of 20,000 unaligned image pairs with both training and test sets. To the best of our knowledge, it is the largest multi-modal SOD dataset, which will advance research on alignment-free RGB-T SOD, saving the labor cost of manual alignment.
- UVT20K covers a wide range of scenes and object categories. As in previous work (Liu et al. 2021a; Wang et al. 2024a), we count and report the total number of scenes and object categories for UVT20K and the compared datasets in Table 1, which suggests that UVT20K has the most variety of scenes and objects. For a more detailed analysis, Fig. 2(a) illustrates the counts of the top 60% scenes and object categories, showing an approximately smooth distribution.
- UVT20K provides a more comprehensive set of annotations, including fully-supervised saliency masks, weakly-supervised scribbles, object boundaries, and challenge attributes. Compared to existing multi-modal SOD datasets that typically involve only saliency mask

annotations, the diverse annotation sets in UVT20K enable the exploration for further research, such as weakly-supervised methods and boundary-enhanced algorithms.

- UVT20K presents significant challenges for exploration. As shown in Table 1, UVT20K has the highest number of challenge types. Fig. 2(c) shows that UVT20K has the largest count within each challenge category, and Fig. 2(b) indicates that each UVT20K sample typically encompasses multiple challenges. In addition, multi-platform shoots at Hikvision and FLIR further intensify the challenges. These challenges will be a valuable asset for assessing the robustness of SOD models.

Methodology

Motivation. For aligned visible-thermal image pairs, the same object is corresponding in space. In this case, the RGB and thermal modalities are inherently correlated, which provides a basis for further exploration of multi-modal complementary information. However, there are positional offsets and scale differences between unaligned image pairs, reducing the modality correlation. Therefore, modeling the corresponding multi-modal correlations is the key to alignment-free RGB-T SOD. To this end, the proposed Progressive Correlation Network (PCNet) first seeks the corresponding regions in unaligned image pairs, and then models the inter- and intra-modal correlations for salient regions.

Overview

The overall architecture of PCNet is illustrated in Fig. 3, which receives a pair of unaligned RGB and thermal images and consists of two parallel encoders, a semantic feature fusion component, a Semantics-guided Homography Estimation (SHE) module, an Inter- and Intra-Modal Correlation (IIMC) module, and a decoder. To be specific, the two encoders (i.e., Swin-B (Liu et al. 2021b)) separately extract multi-level features from the input image pairs (i.e., I_{rgb} and I_t), denoted as f_m^i ($m \in \{rgb, t\}, i = 1, \dots, 4$). The semantic feature fusion component integrates the top extracted features (i.e., f_{rgb}^4 and f_t^4) through attention operation to obtain semantic information (i.e., f_s) embedded in SHE and IIMC. SHE is proposed to predict the corresponding regions between RGB and thermal image pairs based on homography estimation. On this basis, IIMC models inter- and intra-modal correlations specific to salient regions. Then, the decoder integrates the correlated multi-modal and multi-level

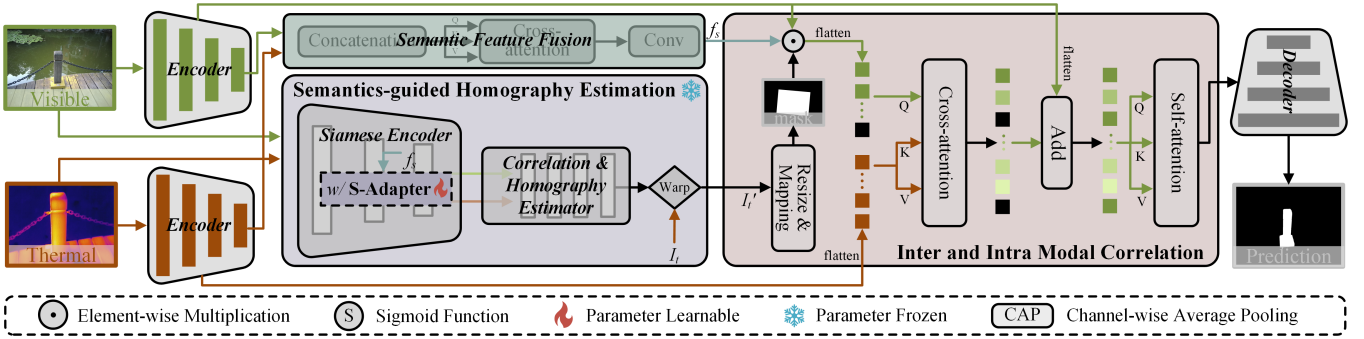


Figure 3: The overall architecture of our proposed Progressive Correlation Network (PCNet). The framework mainly comprises a Semantics-guided Homography Estimation (SHE) module and an Inter- and Intra-Modal Correlation (IIMC) module. SHE is fine-tuned by the S-Adapter to explicitly align the corresponding regions in visible-thermal image pairs. IIMC first models inter-modal correlations for the aligned regions, and then expand the correlations to the whole RGB modality.

features to obtain the final prediction.

Semantics-guided Homography Estimation (SHE)

The same object in unaligned RGB and thermal image pairs is inconsistent in position and scale, resulting in only partial regions correspond to each other. In this case, directly modeling the correlation between the two modalities introduces too much irrelevant information causing noise interference. In order to find the corresponding regions in the RGB and thermal image pairs, we introduce a pre-trained multi-modal homography estimator IHN (Cao et al. 2022), which is structurally simple but effective. However, two issues remain to be solved: 1) the IHN is trained on specific datasets such as the cross-modal GoogleMap dataset (Zhao, Huang, and Zhang 2021), making it difficult to directly deal with RGB-T inputs well, 2) IHN focuses on the entire image region rather than the object region that the SOD task is intended to focus on. To address the two issues, we first introduce the adaptation technique (Houlsby et al. 2019), which is used to fine-tune the pre-trained model to adapt to downstream tasks in a parameter-efficient way. Then, we embed the semantic information that can localize object regions into the adapter to form the proposed Semantic-Adapter (S-Adapter).

To be specific, IHN takes in a pair of source image and target image and outputs the estimated homography matrix H , which can map points in the target image to corresponding points in the source image. As shown in Fig. 3, the main steps of IHN include feature extraction using a siamese encoder, correlation computation, and homography estimation. Considering that the unaligned image pairs are mainly annotated according to the RGB modality, we take the RGB image as the source image and the thermal image as the target image to facilitate the subsequent correlation modeling. The whole process of IHN can be formulated as:

$$H = \mathcal{H}(\Psi(\Phi(I_{rgb}), \Phi(I_t))), \quad (1)$$

where $\Phi(\cdot)$ is the IHN feature encoder, $\Psi(\cdot)$ is the correlation computation function, $\mathcal{H}(\cdot)$ refers to the homography estimator. Then, we embed the S-Adapter into each layer of the encoder for sufficient adaptation:

$$\hat{F}^l = F^l + \text{S-Adapter}_l(F^l, f_s), \quad (2)$$

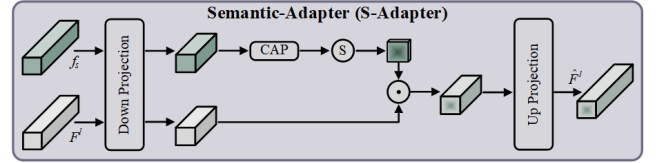


Figure 4: The details of the proposed S-Adapter.

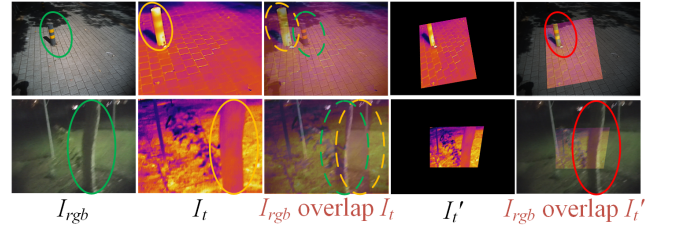


Figure 5: Examples of before and after warping.

where \hat{F}^l is the l_{th} layer adapted feature in the IHN feature encoder, and will be propagated to the next layer.

The detailed flow of S-Adapter is shown in Fig. 4. S-Adapter is in a down-up bottleneck structure, which consists of down-projection, fusion unit \mathcal{G} , ReLU activation ϕ , and up-projection sequentially. In particular, among the fusion unit, the down-projected semantic feature takes its weight distribution as the mask to guide the extracted feature to focus on object regions. The process is formulated as:

$$\text{S-Adapter}_l(F^l, f_s) = \phi(\mathcal{G}(F^l W_{dn}, f_s W_{dn})) W_{up}, \quad (3)$$

$$\mathcal{G}(X, Y) = X \odot \sigma(\text{CAP}(Y)), \quad (4)$$

where W_{dn} and W_{up} are the projection operation, \odot is the element-wise multiplication, σ is the Sigmoid function, and $\text{CAP}(\cdot)$ denotes the channel-wise average pooling.

Then, the process of SHE can be formulated as follows:

$$H = \mathcal{H}(\Psi(\Phi_{\text{Adapter}}(I_{rgb}, f_s), \Phi_{\text{Adapter}}(I_t, f_s))), \quad (5)$$

where $\Phi_{\text{Adapter}}(\cdot)$ is the encoder fine-tuned by the S-Adapter. Finally, the warped thermal image I'_t is obtained using the

estimated homography H :

$$I'_t = \text{Warp}(I_t, H). \quad (6)$$

Fig. 5 shows the visual results of thermal images before and after warping for some examples, indicating that SHE can warp objects for alignment without background interference.

Inter- and Intra-Modal Correlation (IIMC)

The warped thermal image aligns the thermal modality with the corresponding and common areas in the RGB modality. Based on this, IIMC leverages the aligned regions from the warped thermal image to model inter-modal correlations and further expands the correlations to the entire region within the RGB modality. Considering that information loss caused by image warping hinders effective multi-modal fusion (Qin et al. 2023), we use the warped thermal image to map out the corresponding region in the RGB modality, which then interacts with the unwrapped thermal modality. In addition, the semantic information is also introduced to promote the correlation modeling focusing on object regions. The process of the inter-modal correlation modeling can be formulated as:

$$f_{\text{inter}}^i = \mathcal{C}(f_{rgb}^i \odot \mathcal{M}(I'_t) \odot f_s, f_t^i), \quad (7)$$

$$\mathcal{C}(Q, V) = \text{softmax}\left(\frac{QK^T}{\sqrt{d_k}}\right)V + Q, \quad (8)$$

where f_{inter}^i is the inter-modal correlation feature, $\mathcal{M}(\cdot)$ is the mapping and resize operation, and $\mathcal{C}(\cdot)$ represents the transformer-based (Vaswani 2017) correlation operation, in which Q , K , V are queries, keys, and values.

Since only a subset of the region is correlated, the goal is changed to how to expand the correlated region to cover the entire region within the RGB modality. Therefore, we perform intra-modal correlation to supplement the inter-modal correlation results. Specifically, we first attach the inter-modal correlation result f_{inter}^i to the whole RGB modality f_{rgb}^i through residual connection, and then propagate the inter-modal correlation to the whole RGB modality through the correlation operation. Mathematically, the intra-modal correlation is expressed by:

$$f_{\text{intra}}^i = \mathcal{C}(f_{rgb}^i + f_{\text{inter}}^i, f_{rgb}^i + f_{\text{inter}}^i), \quad (9)$$

where f_{intra}^i is the output correlated feature.

Eventually, as in previous works (Liu et al. 2021c; Wang et al. 2024a), the decoder integrates the correlated features in a top-down manner to obtain final predictions, which are supervised by saliency ground-truths and optimized with a combination of binary cross-entropy loss and dice loss.

Experiments

Experiment Setup

Datasets and Evaluation Metrics. To fully evaluate models, we conduct experiments on both aligned and unaligned datasets. For alignment-free models, we train our method and compared methods on the training set of UVT20K and test them on UVT2000, un-VT821, un-VT1000, and the test sets of un-VT5000 and UVT20K. Note that we include

the weakly aligned datasets (i.e., un-VT821, un-VT1000, and un-VT5000) here for comprehensive evaluation. Following previous works (Tu et al. 2021, 2022), we train our alignment-based model on the training set of VT5000 and test on VT821, VT1000, and the test set of VT5000.

We employ three widely used evaluation metrics to assess model performance, including enhanced-alignment E_m , structure-measure S_m , and F-measure F_m .

Implementation Details. Our aligned and unaligned models are implemented on two RTX 3090 GPUs with the same settings. The AdamW optimizer with the learning rate of $1e-5$, weight decay of $1e-4$, batch size of 4, and training epoch of 80 is used to optimize model parameters. The input images are resized to 384×384 during training and inference.

Comparison with State-of-the-Art Methods

We compare our method with 13 state-of-the-art RGB-T SOD methods, including SACNet (Wang et al. 2024a), LAFB (Wang et al. 2024b), CAVER (Pang et al. 2023), LSNet (Zhou et al. 2023), MCFNet (Ma et al. 2023), HRTransNet (Tang et al. 2022), DCNet (Tu et al. 2022), TNet (Cong et al. 2022), OSRNet (Huo et al. 2022), SwinNet (Liu et al. 2021c), CGFNet (Wang et al. 2021), CSRNet (Huo et al. 2021), and MIDD (Tu et al. 2021). To make a fair comparison, we use the results published by the authors or run their released code with default parameters. Table 2 presents the quantitative results, showing that our method achieves optimal performance on all eight datasets, except for a slight weakness on the E_m and F_m metrics of the VT5000 dataset. Compared to the sub-optimal method (i.e., CAVER), our PCNet achieves an improvement of 6.2%, 2.8%, and 7.8% on the three metrics (i.e., E_m , S_m , and F_m) of the two unaligned datasets. It is worth noting that our method has the smallest performance gap between the weakly aligned datasets and their corresponding aligned datasets, further indicating that our method is able to effectively handle misalignment. For example, the average gap between our method on the three metrics for VT5000 and un-VT5000 is 3.8%, while for SACNet, the gap is 9.1%.

Ablation Studies

Effect of SHE. We evaluate the impact of the SHE module by removing it (ID1 in Table 3), which means that correlations are modeled without alignment. Compared to our full model (i.e., ID0), the average decrease is 3.2%, 2.6%, and 4.3% on the three metrics (i.e., E_m , S_m , and F_m) across the two unaligned datasets. It is worth noting that SHE remains valid on the aligned dataset (i.e., VT5000), mainly because the fine-tuned SHE is able to adapt to different inputs and make alignments as needed. ID2 further verifies the effectiveness of the parameter-frozen homography estimator by removing the S-Adapter. The comparison (ID2 vs ID0) demonstrates the positive effect of the S-Adapter. Moreover, the weak performance of ID3 proves that full fine-tuning destroys the ability of the pre-trained homography estimator.

Effect of IIMC. We replace IIMC with feature summation, which implies that the aligned multi-modal features are simply fused. Comparison with the full model (ID4 vs ID0) shows that IIMC improves all metrics. In addition, ID5

Method	MIDD ₂₁	CSRNet ₂₁	CGFNet ₂₁	SwinNet ₂₁	OSRNet ₂₁	TNet ₂₂	DCNet ₂₂	HRTrans ₂₂	MCFNet ₂₃	LSNet ₂₃	CAVER ₂₃	LAFB ₂₄	SACNet ₂₄	PCNet	
UVT20K	$E_m \uparrow$	0.842	0.790	0.819	0.850	0.835	0.876	0.853	0.839	0.875	0.828	0.876	0.858	0.819	0.897
	$S_m \uparrow$	0.836	0.753	0.829	0.841	0.807	0.856	0.808	0.852	0.842	0.834	0.861	0.847	0.829	0.872
	$F_m \uparrow$	0.743	0.635	0.709	0.728	0.730	0.783	0.776	0.710	0.800	0.699	0.790	0.757	0.709	0.822
UVT2000	$E_m \uparrow$	0.727	0.658	0.704	0.780	0.764	0.782	0.808	0.706	0.784	0.711	0.782	0.774	0.792	0.851
	$S_m \uparrow$	0.778	0.655	0.764	0.790	0.741	0.792	0.767	0.758	0.774	0.763	0.786	0.778	0.795	0.819
	$F_m \uparrow$	0.563	0.420	0.539	0.592	0.567	0.610	0.632	0.525	0.621	0.527	0.616	0.594	0.601	0.686
un-VT5000	$E_m \uparrow$	0.885	0.713	0.868	0.901	0.846	0.905	0.879	0.899	0.892	0.892	0.893	0.908	0.899	0.936
	$S_m \uparrow$	0.830	0.642	0.833	0.837	0.800	0.858	0.812	0.872	0.836	0.847	0.850	0.851	0.872	0.879
	$F_m \uparrow$	0.778	0.475	0.757	0.767	0.741	0.807	0.803	0.780	0.809	0.767	0.805	0.803	0.780	0.861
un-VT1000	$E_m \uparrow$	0.884	0.732	0.878	0.871	0.942	0.880	0.880	0.872	0.886	0.875	0.881	0.880	0.868	0.947
	$S_m \uparrow$	0.875	0.705	0.877	0.853	0.980	0.868	0.858	0.869	0.876	0.868	0.873	0.862	0.852	0.922
	$F_m \uparrow$	0.837	0.582	0.817	0.802	0.951	0.827	0.850	0.785	0.850	0.797	0.838	0.824	0.803	0.904
un-VT821	$E_m \uparrow$	0.884	0.783	0.874	0.903	0.848	0.913	0.869	0.901	0.893	0.875	0.856	0.889	0.916	0.936
	$S_m \uparrow$	0.843	0.737	0.837	0.854	0.814	0.876	0.817	0.873	0.850	0.842	0.818	0.834	0.876	0.893
	$F_m \uparrow$	0.791	0.619	0.776	0.783	0.734	0.829	0.793	0.782	0.818	0.754	0.780	0.791	0.812	0.869
VT5000	$E_m \uparrow$	0.897	0.905	0.922	0.942	0.908	0.927	0.920	0.945	0.924	0.915	0.924	0.931	0.957	0.956
	$S_m \uparrow$	0.868	0.868	0.883	0.912	0.875	0.895	0.871	0.912	0.887	0.877	0.892	0.893	0.917	0.920
	$F_m \uparrow$	0.801	0.811	0.851	0.865	0.823	0.846	0.847	0.871	0.848	0.825	0.841	0.857	0.901	0.899
VT1000	$E_m \uparrow$	0.933	0.925	0.944	0.947	0.935	0.937	0.948	0.945	0.944	0.935	0.945	0.945	0.958	0.958
	$S_m \uparrow$	0.915	0.918	0.923	0.938	0.926	0.929	0.922	0.938	0.932	0.925	0.936	0.932	0.942	0.943
	$F_m \uparrow$	0.882	0.877	0.906	0.896	0.892	0.889	0.911	0.900	0.902	0.885	0.903	0.905	0.923	0.924
VT821	$E_m \uparrow$	0.895	0.909	0.912	0.926	0.896	0.919	0.912	0.929	0.918	0.911	0.919	0.915	0.932	0.941
	$S_m \uparrow$	0.871	0.884	0.881	0.904	0.875	0.899	0.876	0.906	0.891	0.878	0.891	0.884	0.906	0.915
	$F_m \uparrow$	0.804	0.831	0.845	0.847	0.814	0.842	0.841	0.853	0.844	0.825	0.839	0.843	0.868	0.879

Table 2: Quantitative comparisons with 13 state-of-the-art RGB-T SOD methods on two unaligned, three weakly aligned, and three aligned datasets. The best results are marked in **bold**.

ID	models	UVT20K			UVT2000			VT5000		
		$E_m \uparrow$	$S_m \uparrow$	$F_m \uparrow$	$E_m \uparrow$	$S_m \uparrow$	$F_m \uparrow$	$E_m \uparrow$	$S_m \uparrow$	$F_m \uparrow$
0	PCNet	0.897	0.872	0.822	0.851	0.819	0.686	0.956	0.920	0.899
1	w/o SHE	0.875	0.849	0.786	0.819	0.800	0.660	0.948	0.915	0.884
2	w/o S-Adapter	0.880	0.856	0.798	0.822	0.806	0.674	0.951	0.914	0.886
3	w/ FFT	0.890	0.865	0.810	0.841	0.813	0.681	0.953	0.917	0.889
4	w/o IIMC	0.864	0.843	0.782	0.817	0.798	0.656	0.943	0.907	0.870
5	w/o Intra	0.877	0.851	0.791	0.831	0.807	0.668	0.947	0.909	0.878
6	w/o Semantics	0.888	0.867	0.804	0.836	0.810	0.679	0.954	0.918	0.894
7	w/o Thermal	0.849	0.831	0.747	0.795	0.788	0.615	0.941	0.904	0.867

Table 3: Ablation analyses of the proposed components. 'w/o': remove the component. 'FFT': full fine-tuning.

shows the results of removing intra-modal correlations, indicating that the progressive modeling approach is effective. **Effect of Semantics.** Since the semantic information is embedded into both SHE and IIMC for guidance, we remove it to verify its effectiveness. The comparison between ID6 and ID0 shows the positive role of the semantic information.

Effect of Thermal Modality. We also replace thermal inputs with corresponding visible images. This implies that our model only uses the RGB modality for prediction. The obvious performance drop in ID7 proves that the unaligned thermal modality can provide effective complementary information through correlation modeling. In addition, the drop on the unaligned datasets is greater than that on the aligned datasets, suggesting that the RGB images in the unaligned dataset are more challenging and rely on the thermal modality as information supplement.

Effect of UVT20K. We further analyze the effectiveness of the proposed UVT20K dataset by comparing the model performance of using the other training set. As in work (Wang et al. 2024a), we train our model and some recent advanced models using the training set of un-VT5000. For a fair comparison, we only evaluate them on the UVT2000 dataset instead of the test sets of UVT20K or un-VT5000 with the

Training Set	UVT20K			un-VT5000		
Test set	UVT2000			UVT2000		
Metric	$E_m \uparrow$	$S_m \uparrow$	$F_m \uparrow$	$E_m \uparrow$	$S_m \uparrow$	$F_m \uparrow$
PCNet (Ours)	0.851	0.819	0.686	0.799	0.813	0.646
CAVER (Pang et al. 2023)	0.782	0.786	0.616	0.727	0.749	0.535
LSNet (Zhou et al. 2023)	0.711	0.763	0.527	0.679	0.728	0.478
MCFNet (Ma et al. 2023)	0.784	0.774	0.621	0.727	0.739	0.535

Table 4: Comparison of models using different training sets.

same distribution. The results in Table 4 show that the model trained with the large-scale UVT20K has significant performance advantages, indicating that UVT20K contributes to the research of alignment-free RGB-T SOD. Moreover, the optimal performance on both training sets demonstrates the generalization of our method.

Conclusion

In this paper, we construct a large-scale dataset UVT20K for alignment-free RGB-T SOD. To the best of our knowledge, UVT20K is the largest multi-modal SOD dataset, containing 20,000 samples divided into training and test sets. It covers a wide range of scenes and object categories, offers a comprehensive set of annotations, and presents significant challenges. With these features, the UVT20K will make significant contributions to research on RGB-T SOD and unaligned image pairs. In addition, we propose a Progressive Correlation Network (PCNet) that aligns the corresponding regions and successively models inter-modal and intra-modal correlations for accurate saliency predictions in unaligned image pairs. Extensive experiments demonstrate the potential of the proposed UVT20K dataset and the effectiveness of our method. In future work, we will explore more challenges in unaligned image pairs, such as varying camera viewpoints and inconsistent image depth of field.

Acknowledgments

This work was in part supported by the University Synergy Innovation Program of Anhui Province (No. GXXT-2022-014), the National Natural Science Foundation of China (No. 62376004 and No. 62376005), and the Natural Science Foundation of Anhui Province (NO. 2208085J18).

References

- Cao, S.-Y.; Hu, J.; Sheng, Z.; and Shen, H.-L. 2022. Iterative deep homography estimation. In *Proceedings of the IEEE/CVF conference on computer vision and pattern recognition*, 1879–1888.
- Cong, R.; Zhang, K.; Zhang, C.; Zheng, F.; Zhao, Y.; Huang, Q.; and Kwong, S. 2022. Does thermal really always matter for RGB-T salient object detection? *IEEE Transactions on Multimedia*, 25: 6971–6982.
- Fan, D.; Wang, W.; Cheng, M.; and Shen, J. 2019. Shifting More Attention to Video Salient Object Detection. In *IEEE Conference on Computer Vision and Pattern Recognition*, 8554–8564.
- Fan, D.-P.; Lin, Z.; Zhang, Z.; Zhu, M.; and Cheng, M.-M. 2020. Rethinking RGB-D salient object detection: Models, data sets, and large-scale benchmarks. *IEEE Transactions on neural networks and learning systems*, 32(5): 2075–2089.
- Houlsby, N.; Giurgiu, A.; Jastrzebski, S.; Morrone, B.; De Laroussilhe, Q.; Gesmundo, A.; Attariyan, M.; and Gelly, S. 2019. Parameter-efficient transfer learning for NLP. In *International Conference on Machine Learning*, 2790–2799. PMLR.
- Huo, F.; Zhu, X.; Zhang, L.; Liu, Q.; and Shu, Y. 2021. Efficient context-guided stacked refinement network for RGB-T salient object detection. *IEEE Transactions on Circuits and Systems for Video Technology*, 32(5): 3111–3124.
- Huo, F.; Zhu, X.; Zhang, Q.; Liu, Z.; and Yu, W. 2022. Real-time one-stream semantic-guided refinement network for RGB-thermal salient object detection. *IEEE Transactions on Instrumentation and Measurement*, 71: 1–12.
- Li, S.; Xu, M.; Ren, Y.; and Wang, Z. 2017. Closed-form optimization on saliency-guided image compression for HEVC-MSP. *IEEE Transactions on Multimedia*, 20(1): 155–170.
- Liu, N.; Zhang, N.; Shao, L.; and Han, J. 2021a. Learning selective mutual attention and contrast for RGB-D saliency detection. *IEEE Transactions on Pattern Analysis and Machine Intelligence*, 44(12): 9026–9042.
- Liu, Z.; Lin, Y.; Cao, Y.; Hu, H.; Wei, Y.; Zhang, Z.; Lin, S.; and Guo, B. 2021b. Swin transformer: Hierarchical vision transformer using shifted windows. In *Proceedings of the IEEE/CVF international conference on computer vision*, 10012–10022.
- Liu, Z.; Tan, Y.; He, Q.; and Xiao, Y. 2021c. SwinNet: Swin transformer drives edge-aware RGB-D and RGB-T salient object detection. *IEEE Transactions on Circuits and Systems for Video Technology*, 32(7): 4486–4497.
- Lu, A.; Li, C.; Yan, Y.; Tang, J.; and Luo, B. 2021. RGBT tracking via multi-adapter network with hierarchical divergence loss. *IEEE Transactions on Image Processing*, 30: 5613–5625.
- Ma, S.; Song, K.; Dong, H.; Tian, H.; and Yan, Y. 2023. Modal complementary fusion network for RGB-T salient object detection. *Applied Intelligence*, 53(8): 9038–9055.
- Pang, Y.; Zhao, X.; Zhang, L.; and Lu, H. 2023. CAVER: Cross-Modal View-Mixed Transformer for Bi-Modal Salient Object Detection. *IEEE Trans. Image Process.*, 32: 892–904.
- Piao, Y.; Ji, W.; Li, J.; Zhang, M.; and Lu, H. 2019. Depth-induced multi-scale recurrent attention network for saliency detection. In *Proceedings of the IEEE/CVF international conference on computer vision*, 7254–7263.
- Qin, Z.; Chen, J.; Chen, C.; Chen, X.; and Li, X. 2023. Uni-fusion: Unified multi-view fusion transformer for spatial-temporal representation in bird’s-eye-view. In *Proceedings of the IEEE/CVF International Conference on Computer Vision*, 8690–8699.
- Tang, B.; Liu, Z.; Tan, Y.; and He, Q. 2022. HRTransNet: HRFormer-driven two-modality salient object detection. *IEEE Transactions on Circuits and Systems for Video Technology*, 33(2): 728–742.
- Tang, J.; Fan, D.; Wang, X.; Tu, Z.; and Li, C. 2019. RGBT salient object detection: Benchmark and a novel cooperative ranking approach. *IEEE Transactions on Circuits and Systems for Video Technology*, 30(12): 4421–4433.
- Tu, Z.; Li, Z.; Li, C.; Lang, Y.; and Tang, J. 2021. Multi-interactive dual-decoder for RGB-thermal salient object detection. *IEEE Transactions on Image Processing*, 30: 5678–5691.
- Tu, Z.; Li, Z.; Li, C.; and Tang, J. 2022. Weakly alignment-free RGBT salient object detection with deep correlation network. *IEEE Transactions on Image Processing*, 31: 3752–3764.
- Tu, Z.; Ma, Y.; Li, Z.; Li, C.; Xu, J.; and Liu, Y. 2020. RGBT Salient Object Detection: A Large-scale Dataset and Benchmark. *CoRR*, abs/2007.03262.
- Tu, Z.; Xia, T.; Li, C.; Wang, X.; Ma, Y.; and Tang, J. 2019. RGB-T image saliency detection via collaborative graph learning. *IEEE Transactions on Multimedia*, 22(1): 160–173.
- Vaswani, A. 2017. Attention is All You Need. *arXiv preprint arXiv:1706.03762*.
- Wang, G.; Li, C.; Ma, Y.; Zheng, A.; Tang, J.; and Luo, B. 2018. RGB-T saliency detection benchmark: Dataset, baselines, analysis and a novel approach. In *Image and Graphics Technologies and Applications: 13th Conference on Image and Graphics Technologies and Applications, IGTA 2018, Beijing, China, April 8–10, 2018, Revised Selected Papers 13*, 359–369. Springer.
- Wang, J.; Song, K.; Bao, Y.; Huang, L.; and Yan, Y. 2021. CGFNet: Cross-guided fusion network for RGB-T salient object detection. *IEEE Transactions on Circuits and Systems for Video Technology*, 32(5): 2949–2961.

- Wang, K.; Lin, D.; Li, C.; Tu, Z.; and Luo, B. 2024a. Alignment-Free RGBT Salient Object Detection: Semantics-guided Asymmetric Correlation Network and A Unified Benchmark. *IEEE Transactions on Multimedia*.
- Wang, K.; Tu, Z.; Li, C.; Zhang, C.; and Luo, B. 2024b. Learning Adaptive Fusion Bank for Multi-modal Salient Object Detection. *IEEE Transactions on Circuits and Systems for Video Technology*.
- Wang, W.; Lai, Q.; Fu, H.; Shen, J.; Ling, H.; and Yang, R. 2022. Salient Object Detection in the Deep Learning Era: An In-Depth Survey. *IEEE Trans. Pattern Anal. Mach. Intell.*, 44(6): 3239–3259.
- Yuan, M.; Shi, X.; Wang, N.; Wang, Y.; and Wei, X. 2024. Improving RGB-infrared object detection with cascade alignment-guided transformer. *Information Fusion*, 105: 102246.
- Zhang, P.; Liu, W.; Wang, D.; Lei, Y.; Wang, H.; and Lu, H. 2020. Non-rigid object tracking via deep multi-scale spatial-temporal discriminative saliency maps. *Pattern Recognit.*, 100: 107130.
- Zhao, Y.; Huang, X.; and Zhang, Z. 2021. Deep lucaskanade homography for multimodal image alignment. In *Proceedings of the IEEE/CVF conference on computer vision and pattern recognition*, 15950–15959.
- Zhou, W.; Zhu, Y.; Lei, J.; Yang, R.; and Yu, L. 2023. LSNet: Lightweight spatial boosting network for detecting salient objects in RGB-thermal images. *IEEE Transactions on Image Processing*, 32: 1329–1340.
- Zhu, Y.; Li, C.; Tang, J.; Luo, B.; and Wang, L. 2021. RGBT tracking by trident fusion network. *IEEE Transactions on Circuits and Systems for Video Technology*, 32(2): 579–592.